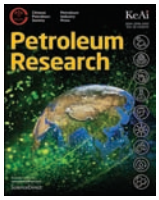
Petroleum Research 11 (2026) 150–162

Contents lists available at ScienceDirect

Petroleum Research

journal homepage: http://www.keaipublishing.com/en/journals/petroleum-research/



Full Length Article

Computation of pressure depletion and well productivity of multi-fractured wells with variable fracture spacing using fast and accurate solution method



Yakai Tian [a,b], Ruud Weijermars [a,c,*]

[a] Department of Petroleum Engineering, College of Petroleum Engineering and Geosciences (CPG), King Fahd University of Petroleum & Minerals (KFUPM), Dhahran, 31261, Saudi Arabia
[b] PetroChina Research Institute of Petroleum Exploration and Development (RIPED), Beijing 100083, China
[c] Center for Integrative Petroleum Research (CIPR), College of Petroleum Engineering and Geosciences (CPG), King Fahd University of Petroleum & Minerals (KFUPM), Dhahran, 31261, Saudi Arabia

ARTICLE INFO

Article history:
Received 6 November 2024
Received in revised form
27 August 2025
Accepted 27 August 2025
Available online 2 September 2025

Keywords:
Coupled pressure-superposition method
Gaussian pressure transients
Pressure interference
History matching
Eagle Ford

ABSTRACT

This study presents a fast method that can model the pressure depletion around hydraulically fractured wells accurately. The Gaussian Pressure-Transient (GPT) method has infinite resolution, because no discrete-grid computations are required – the method solves the pressure field using closed-form solutions. After extensive testing on field cases and calibration against other (independent) solution-methods, it appeared that the pressure interference of multiple fractures represented by pressure transients – in the early phases of pressure advance – behaves according to the traditional superposition-method. However, when pressure interference advances, the traditional superposition method gives increasingly unrealistic and inaccurate results. Therefore, the traditional superposition method typically used for steady-state, needs adjustment when applied to transient systems, modeled here with Gaussian pressure-diffusion probability-density functions. The new solutions are valid for the advance of pressure changes both in the early and late stages of the well-life. A second new insight presented here is that the superposition of multiple fractures using Gaussian solutions (together with pressure-gradient computations and application of Darcy's) can accurately forecast the future production rate and cumulative production of the well over the economic well-life, accounting for the impact of fracture-spacing changes. The new method is validated by history-matching of our Gaussian forecasts using real well-data to constrain specific reservoir properties (hydraulic diffusivity) and completion parameters (fracture half-lengths), and then was benchmarked against independent simulations with CMG-IMEX.

© 2025 Chinese Petroleum Society. Publishing services by Elsevier B.V. on behalf of KeAi Communications Co. Ltd. This is an open access article under the CC BY license (http://creativecommons.org/licenses/by/4.0/).

1. Introduction

Geological reservoirs are intensively exploited for energy extraction (hydrocarbons, geothermal fluids), groundwater sourcing, and for either temporary or long-term storage of fluids by injection (such as hydrogen, carbon-dioxide sequestration, and produced water) (Guo et al., 2023). This study outlines fast and accurate new solution paths (closed-form) that have come of age to model fluid flow in subsurface reservoirs and offer considerable advantages over traditional reservoir modeling tools (numerical). The Gaussian Pressure-Transient (GPT) method has been successfully used in a variety of applications, including the study of pressure-induced stress-reversals during hydraulic fracturing (Wang and Weijermars, 2021), and competition between molecular diffusion and pressure diffusion in shale gas reservoirs (Afagwu et al., 2024; Weijermars and Afagwu, 2022). This study presents new algorithms and results using a novel closed-form reservoir-modeling tool based on the recently developed Gaussian Pressure-Transient (GPT) solutions. A brief review is given below to place the various approaches (numerical and closed-form) in perspective.

* Corresponding author. Department of Petroleum Engineering, College of Petroleum Engineering and Geosciences (CPG), King Fahd University of Petroleum & Minerals (KFUPM), Dhahran, 31261, Saudi Arabia.
E-mail address: ruud.weijermars@kfupm.edu.sa (R. Weijermars).
Peer review under the responsibility of Editorial Office of Petroleum Research.

https://doi.org/10.1016/j.ptlrs.2025.08.008
2096-2495/© 2025 Chinese Petroleum Society. Publishing services by Elsevier B.V. on behalf of KeAi Communications Co. Ltd. This is an open access article under the CC BY license (http://creativecommons.org/licenses/by/4.0/).

Numerical solutions: Mainstream solution methods (widely used in both industry and academia) for modeling pressure depletion (production wells) and pressure increases (injection wells) and the associated flow in subsurface reservoirs are based on discrete element computations. Under the commercial reservoir simulators, widely applied by industry in conventional reservoirs, are CMG-IMEX, an industry-standard black-oil simulator; compositional simulator GEM and a thermal compositional simulator STARS. KAPPA-Rubis is a numerical simulator from KAPPA petroleum engineering software, which also offers a Decline Curve Analysis (DCA) module (Citrine), Pressure Transient Analysis (PTA) module (Saphir), and Rate Transient Analysis (RTA) module (Topaz) (Bai et al., 2024; Clarkson, 2012).

Eclipse is a commercial reservoir simulator, originally developed by Exploration Consultants Limited and currently owned by Schlumberger; Intersect is a high-performance simulator jointly developed by Schlumberger, Chevron and Total, with the commercial rights owned by Schlumberger. Numerous additional commercial platforms for reservoir modeling of conventional fields exist, such as Echelon, a high-performance reservoir simulator jointly developed by Stone Ridge Technology (SRT) and Eni (commercial rights are owned by SRT), and tNavigator, a high-performance reservoir-simulator developed by Rock Flow Dynamics. Nexus is a simulator originally developed by Amoco and currently owned by Landmark graphics.

Commonly used numerical solution methods for fluid-solid coupling problems include finite difference methods (FDM) (Wang et al., 2022), finite volume methods (FVM) (Lei et al., 2024; Wang et al., 2023), and finite element methods (FEM) (Zhang et al., 2022). Reservoir model plug-ins for complex fracture networks have recently become available, such as Embedded Discrete Fracture Models (EDFM) to explore the degrees of connectivity of the complex spatial distributions of natural fractures for import in CMG to conduct sensitivity studies of well performance (Yu et al., 2021). Simulators previously developed for conventional reservoirs have their merits for modeling the performance of hydraulically fractured well systems, but continue to compete for market share with integrated fracture-simulation/production-modeling software platforms (e.g., ResFrac).

Flow-physics based models may be based on either proprietary codes, or open source codes such as the MATLAB Reservoir Simulation Toolbox (MRST), which provides new solutions based on unstructured grids that can be applied to large and complex systems (Lie, 2019). The Black Oil Applied Simulation Tool (BOAST) is an IMPES, (finite-difference implicit pressure-explicit saturation) numerical simulator which finds the pressure distribution for a given time step first, and then calculates the saturation distribution for the same time step (Fanchi et al., 1982). The Open Porous Media (OPM) initiative is supported by Equinor and provides open source tools and methods for upscaling and simulating fluid flow in porous media (Alvestad, 2021).

Numerical simulators are capable of providing flow simulations while accounting for complex heterogeneity of subsurface geology and multi-phase fluids. Although grid-construction in such numerical models used to be cumbersome, many improvements have been made (unstructured grids, etc.). Nonetheless, for cases with sparse subsurface data (such is invariably the case in the early stages of field development), the complexity and costly computation times of numerical simulators are arguably less practical for the rapid iteration and history-matching of early field data (Ji et al., 2017). Therefore, there still is a niche to fill for solution tools and methods to model subsurface flow: closed-form solutions are invariably faster than simulations based on discrete element computations. Another reason for using closed-form solution methods is that these require neither gridding nor upscaling, which ensures infinite resolution in combination with fast computation times (Ji et al., 2017).

Closed-form solutions: To overcome the constraints of grid-based solutions, alternative solution-methods (other than discrete element computations) have been developed. For multi-fracture horizontal wells (MFHW), some researchers claimed the rectangular drainage area is more in line with the actual situation on site, and linear flow is the main flow mechanism during the well productive life. Brown et al. (2011) utilized the tri-linear concept of Lee and Brockenbrough (1988) and proposed a "tri-linear flow" model, which divides the reservoir into three regions: USRV region, SRV region, and HF region to study the transient pressure response of MFHW. Subsequently, the five-linear model Stalgorova and Mattar (2012) and the seven-linear model (Yuan et al., 2012) were proposed to analyze the pressure response and production performance of complex fracture networks. The linear flow and seepage models of MFHW employ a Laplace transformation, perturbation method and Stehfest numerical inversion (Ji et al., 2017). However, the pressure distribution in the various drainage regions is solved independently, with impractical sudden pressure jumps across flow boundaries, which precludes the calculation of accurate well rates.

Complex Analysis Methods (CAM) have been developed to sidestep many of the aforementioned computational simplifications. The CAM code has been successfully used to model the flow paths and drained rock volume (DRV, or fluid withdrawal) around hydraulically fractured wells, accounting for natural fractures. The CAM results have been visualized and history-matched using independent solution methods using commercial simulators (Khanal and Weijermars, 2019; Nandlal et al., 2020; Parsegov et al., 2018; van Harmelen and Weijermars, 2018; Weijermars et al., 2020a). One of the strengths of CAM models is that flow near discrete fractures can be studied and visualized in great detail (Weijermars et al., 2019).

The insight from CAM models was subsequently applied to develop a so-called flow-cell model (FCM), which is a spreadsheet-coded solver to forecast well productivity with physics-based adjustments to the flow-cells (well-spacing, fracture-spacing, fracture half-length, height and well length) using a type-curve (Weijermars and Khanal, 2019). The FCM-based solutions were extensively tested using real well data (oil, dry gas, wet gas) from US shale basins and benchmarked against independent production forecasting tools (Eclipse, Kappa, CMG, ResFrac), which confirmed the accuracy of the solutions (Waters and Weijermars, 2021). One drawback of CAM-solutions is that these are intrinsically limited to the description of steady-state flow problems. Transient flow which dominates the early well behavior can be approximated by time-stepping and superposing CAM-solutions (Van Harmelen and Weijermars, 2018). But the superposition of such time-stepped steady-state solutions becomes computationally complex again. This time-stepped superposition is no longer needed in a recently developed approach where the pressure changes in the reservoir are modeled using Gaussian Pressure Transients (GPT) (Weijermars, 2021, 2022). The GPT solution method is grid-less, which provides infinite resolution and therefore has superior accuracy as compared to any other solution method (Ji et al., 2023), and GPT solutions have been benchmarked against independent solution methods (Weijermars, 2021; Weijermars and Afagwu, 2022).

The present study takes the analysis using GPT-based solutions a fundamental step further, by critically assessing how pressures from multiple sources are interfering (Section 2). This has led us to a new insight that the traditional pressure-superposition method becomes inaccurate during later runtimes when used to solve pressure-transient problems. A new coupled pressure-

superposition method is proposed, and validated against independent solution methods. The well rates of MFHW can be fast and accurately calculated based on the pressure gradient of the coupled GPT model (Section 3). Application of GPT-solutions to real well data is given (Section 4), followed by a discussion (Section 5) and conclusions (Section 6).

2. Reservoir pressure changes

Modeling fluid flow in subsurface reservoirs in petroleum engineering applications aims to quantify and predict how well-interventions will affect the pressure-change process. Such interventions lead to pressure depletion in the reservoir due to fluid withdrawal, and pressure-increase when fluid injection is applied. Once the pressure everywhere in the reservoir is solved, the pressure gradient can be utilized to determine the local flow direction and flow rate. While the individual computational steps are well-known, our work revealed that for transient pressure changes in the reservoir, the traditional superposition method becomes increasingly inaccurate for larger run-times. Examples are given, after first systematically developing our fundamentally new approach that forms the basis for proposing an improved pressure-superposition method. The new pressure superposition scheme must be used when multiple wells, or a single well with multiple fractures acting as individual pressure-change sources, drain or fill a reservoir with pressure interference. Such interference of the pressure transients originating from different sourcess must be simultaneously accounted for in the model computations.

2.1. Revisiting the pressure transient solution

Consider one vertical hydraulic fracture at the onset of production which imposes a constant pressure, P_{BH}, which acts as a pressure diffusion source for the adjacent reservoir with original pressure, P_0. Taking the (y, z)-plane of the reference frame to coincide with the fracture, the pressure state, $P(x, t)$, at location x in the reservoir space and for time t in the reservoir life since the onset of the pressure disturbance is given by:

$$P(x,t) = P_0 + \Delta P(x,t) \tag{1}$$

Eq. (1) assumes an uni-directional diffusion of the pressure disturbance, ΔP, normal to a planar source (1D-diffusion) of the pressure differential ΔP (0,0) applied in the fracture. This pressure differential propagates into the reservoir space by pressure diffusion, which is compactly represented in the 1D-diffusivity equation (Crank, 1975; Weijermars, 2021):

$$\frac{\partial^2 \Delta P}{\partial x^2} = \frac{1}{D_h}\frac{\partial \Delta P}{\partial t} \tag{2}$$

Rearranging Eq. (1) and introducing a probability function, $p(x, t)$, we may assume a solution of Eq. (2) is given by:

$$\Delta P(x,t) = P(x,t) - P_0 = (P_{BH} - P_0)p(x,t) \tag{3}$$

Revisiting the classic textbook by Crank (1975) with mathematical solutions for a variety of diffusion cases, it appears that the applicable solution for 1D-diffusion into a semi-infinite medium with a constant physical quantity on one side of the half-space is given by the following Gaussian probability function, $p(x, t)$:

$$p(x,t) = 1 - erf\frac{x}{2\sqrt{D_h t}} \tag{4}$$

The probability function $p(x, t)$ has a specific physical meaning, namely corresponding to values of the pressure change everywhere in the reservoir, normalized by the initial reservoir pressure, as becomes immediately obvious from re-arranging Eq. (3):

$$p(x,t) = \frac{\Delta P(x,t)}{\Delta P_0} \tag{5}$$

with $\Delta P_0 = P_{BH} - P_0$.

However, the Gaussian solution of Eq. (4) for the pressure diffusion Eq. (2) can give us the dimensional pressure-change, when multiplied by the initial pressure change in the reservoir $p(x, t)\Delta P_0$. After normalization, as in Eq. (5), the dimensionless pressure change is obtained, which shows how the initial pressure P_0 of the reservoir will be changed by the presence of the fractured well with planar sources of pressure disturbance. The advance of the pressure change in the reservoir space due to the fractures is graphed for different times in Fig. 1, according to Eq. (4). Diffusivity used is 1 and curves shown are for steps of 5 time-units and arbitrary non-dimensional time ranging between 0 and 100.

More precisely, Fig. 1a shows an injection well case, with $P_{BH} > P_0$, such that the $p(x, t)$ of Eq. (5) is a positive probability function, for which case Fig. 1a has the correct sign. The original reservoir pressure is unchanged at $y = 0$, at the lower border of the graph of Fig. 1a, with a dimensional value of P_0, which remains constant and unchanged for $t \leq 0$. However, for $t > 0$, the active injection will change the initial reservoir pressure as indicated by the curves in Fig. 1a. For example, for $t \to \infty$, the pressure in the reservoir will everywhere have attained the non-dimensional pressure-change value of $+1$, which corresponds to a dimensional pressure value of P_{BH} for an injection well.

For the production well case, $P_{BH} < P_0$, such that the $p(x, t)$ of Eq. (5) is better replaced by a negative probability function:

$$p(x,t) = \frac{\Delta P(x,t)}{|\Delta P_0|} = erf\left(\frac{x}{2\sqrt{D_h t}}\right) - 1 \tag{6}$$

Such a negative probability function is a prime example that natural processes are sometimes aptly described by negative probabilities, something argued already in a seminal paper by Feynman (1952). Fig. 1b graphs the production well case, where the original reservoir pressure is unchanged at $y = 0$, at the top border, with a dimensional value of P_0, which remains constant and unchanged for $t \leq 0$. However, for $t > 0$, the active production will change the initial reservoir pressure as indicated by the curves in Fig. 1b. For example, for $t \to \infty$, the pressure in the reservoir will everywhere have attained the non-dimensional pressure-change value of -1, which corresponds to a dimensional pressure value of P_{BH} for a production well.

2.2. Dimensional pressure-transient solutions

If we revert to Eq. (1) and use for $\Delta P(x, t)$ the Gaussian solution of Eqs. (4) and (5) we immediately see that the dimensional pressure state, $P(x, t)$, anywhere in the reservoir at location x, and at any one-time t, is given by the initial reservoir pressure, P_0, and the added change due to the engineering intervention of drilling the well with the changed bottom-hole pressure:

$$P(x,t) = P_0 + (P_{BH} - P_0)\left(1 - erf\left(\frac{x}{2\sqrt{D_h t}}\right)\right) \tag{7}$$

Eq. (7) describes how the original reservoir pressure, P_0, becomes progressively affected by the well pressure as it diffuses into the ambient reservoir space. Interestingly, the same pressure solution can be obtained, rearranging Eq. (7) such that the focus is on

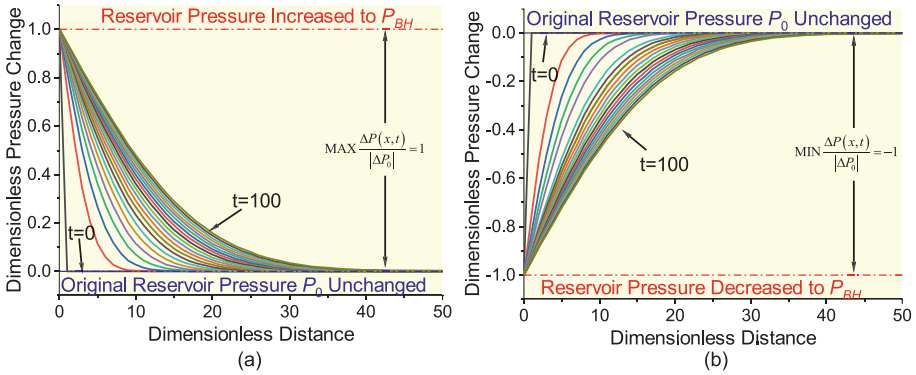


Fig. 1. Normalized pressure-change for (a) Injection well case, according to Eq. (4). b) Production well case, according to Eq. (4).

how the bottom-hole pressure P_{BH} of the fracture will advance into the reservoir space:

$$P(x,t) = P_{BH} + (P_0 - P_{BH})\, erf\left(\frac{x}{2\sqrt{D_h t}}\right) \tag{8}$$

Eq. (7) uses the original reservoir pressure, P_0, as the reference, while Eq. (8) uses the bottom-hole pressure, P_{BH}, as a reference. However, Eqs. (7) and (8) are mathematically identical.

In order to help better understand how the non-dimensional results of Fig. 1a and b translate to dimensional values, specific examples are given in Fig. 2a and b. We assumed an infinite reservoir with an initial pressure of 5000 psi. If there is an injection well with constant bottom pressure of 9000 psi, or a production well with constant bottom pressure of 1000 psi, Fig. 2 shows how the presence of the well affects the initial state P_0 of the reservoir according to Eq. (1). If time is long enough, the pressure near the well will continue to evolve and changes the pressure inside the reservoir asymptotically, as controlled by the advance of the pressure transients, until the finite reservoir space is equalized to the bottomhole pressure after infinite time.

2.3. Traditional pressure-superposition method

Based on the pressure solutions of Eqs. (7) and (8), it is possible to critically examine the traditional method for superposing the pressure disturbance due to the presence of multiple hydraulic fractures in a single well. We found the traditional method gives physically unsound results (see later in this section), which is why we propose a new, coupled pressure-superposition method (Section 2.4).

We initially assumed that for the superposition of pressure changes due to multiple pressure change sources, such as in an array of hydraulic fractures acting as pressure-change sources, the pressure change [starting out from Eq. (1)] would be given by:

$$P(x,t) = P_0 + \sum_{k=1}^{n} \Delta P(x_k, t_k) \tag{9}$$

With $\Delta P(x_k,t_k)$ representing the individual contributions of each pressure-change source k. The hydraulic diffusivity, D_h, captures the intrinsic properties of the reservoir and as all the wells are supposed to interfere in the same reservoir, we assume no variation of the hydraulic diffusivity may occur in the homogeneous reservoir space between the fractures. Furthermore, an instantaneously applied bottom-hole pressure, P_{BH}, is assumed to be held constant in all fractures of the well throughout the production period, as would be reasonable when the well is on pump.

According to the Gaussian probability function (Eq. (4)) of a single fracture and applying traditional pressure superposition method (Eq. (9)), the pressure distribution equation in a multi-fracture reservoir can be obtained as:

$$P(x,t) = P_0 + (P_{BH} - P_0) \sum_{k=1}^{n} \left(1 - erf\left(\frac{x_k}{2\sqrt{D_h t_k}}\right)\right) \tag{10}$$

From Eq. (10), the pressure change distribution probability function of multi-fracture reservoir can be obtained as:

$$p(x,t) = \sum_{k=1}^{n} \left(1 - erf\left(\frac{x_k}{2\sqrt{D_h t_k}}\right)\right) \tag{11}$$

Fig. 3 shows an example of the pressure changes between two adjacent hydraulic fractures which are part of a production well, newly inserted in the reservoir space. The pressure-change curves

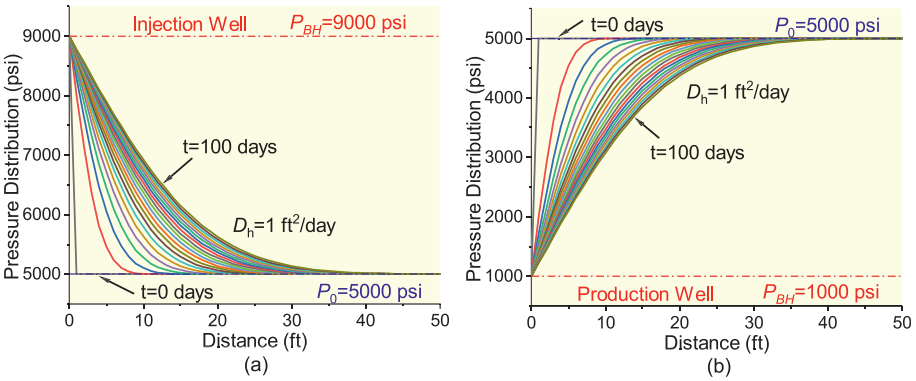


Fig. 2. Reservoir pressure field evolution curves for (a) Injection well, b) Production well. D_h = 1 ft^2/day.

are given for twelve successive times (see legend), according to the traditional superposition method of Eq. (9) (D_h = 1 ft^2/day). The dashed horizontal lines represent (1) the original reservoir pressure (top dashed line), (2) the bottom-hole pressure (middle dashed line), and (3) the zero reservoir-pressure level (bottom dashed line). The fractures, with P_{BH} = 1000 psi, will over time lower the original reservoir pressure (P_0 = 5000 psi), which is in Fig. 3 shown for an assumed hydraulic diffusivity (D_h = 1 ft^2/day). The pressure drawdown is shown after 20–1000 days since the onset of production, with the fractures acting as the sole sources of the progressive pressure perturbation.

However, applying the superposition according to Eq. (9), termed here the traditional method, we discovered after finite times, the pressure may either drop below the bottom-hole pressure (in case of production) or exceed the bottom-hole pressure (in case of injection). This limitation of the traditional pressure superposition method was already signaled in an earlier study of our group (Alotaibi et al., 2023), due to which a runtime limit needed to be used to prevent the pressure from becoming non-physical (i.e. not attaining a value beyond the bottom-hole pressure). The non-physicality of the traditional pressure superposition method of Eq. (9) becomes very clear when the production time is long enough: the calculated reservoir pressure will asymptotically go to −3000 psi; the dimensionless pressure change will asymptotically go to −2. The implication of the simple example of Fig. 3 is that the traditional pressure superposition method will cause the pressure to exceed the difference between the bottom-hole pressure and the reservoir pressure, which is against the laws of physics. The reservoir pressure may never drop below the bottom-hole pressure of 1000 psi, which was the initial P_{BH} imposed in the example of Fig. 3.

We subsequently endeavored to correct the pressure superposition model by using a coupled method, newly proposed here, where a runtime limit is no longer needed. The derivation of our new, coupled pressure-superposition method is given below (Section 2.4).

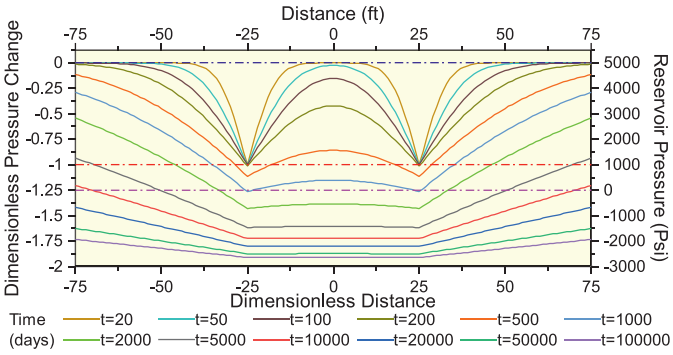


Fig. 3. Dimensionless pressure-change plot and reservoir pressure distribution for reservoir space containing two hydraulic fractures placed at $x = -25$ ft and $x = +25$ ft, respectively, and spaced 50 ft. Pressure plot is valid for orientation perpendicular to the vertical fractures.

2.4. Coupled pressure-superposition method

The traditional pressure superposition model treats each fracture as an independent source, which results in a doubling of the pressure changes. Key steps in designing the improved, coupled superposition method are explained in Appendix A, using examples of 2 and 3 fracture pressure-change sources.

For a reservoir with n wells or fractures, the coupled pressure superposition method when a reservoir-pressure-centric approach is taken (as in Eqs. (1)–(3)) is as follows:

$$P(x_{\Sigma n}, t_{\Sigma n}) = P_0 + \Delta P_0 \times \left(\frac{\Delta P(x_{\Sigma n-1}, t_{\Sigma n-1})}{\Delta P_0} + \frac{\Delta P(x_n, t_n)}{\Delta P_0} - \frac{\Delta P(x_{\Sigma n-1}, t_{\Sigma n-1}) \times \Delta P(x_n, t_n)}{\Delta P_0^2} \right) \tag{12}$$

with $\Delta P(x_{\Sigma n-1}, t_{\Sigma n-1}) = P(x_{\Sigma n-1}, t_{\Sigma n-1}) - P_0$.

$\Delta P(x_n, t_n)$ is the pressure change caused by a single fracture n, while $\Delta P(x_{\Sigma n-1}, t_{\Sigma n-1})$ is the pressure change previously caused by the other fractures.

Now consider the relatively simple case of two adjacent factures, contributing to pressure change in the reservoir at the same time. When only two fractures are involved, the pressure change in the reservoir space between the fractures is given by:

$$P(x,t) = P_0 + \Delta P_0 \times \left(\frac{\Delta P(x_1, t_1)}{\Delta P_0} + \frac{\Delta P(x_2, t_2)}{\Delta P_0} - \frac{\Delta P(x_1, t_1) \times \Delta P(x_2, t_2)}{\Delta P_0^2} \right) \tag{13}$$

It can be seen from Eq. (12) and Eq. (13) that the new pressure superposition model differs from the traditional pressure superposition model of Eq. (9) in that a correction coefficient is added (the final term in Eq. (13)), which accounts for the pressure interference between fractures. The fracture-pair will act as two different, effective diffusion sources with rates $\left(1 - erf \frac{x_1}{2\sqrt{D_h t}}\right)$ and $\left(1 - erf \frac{x_2}{2\sqrt{D_h t}}\right)$, respectively. Now assume Fracture 1 is located at (x_a, y), such that $x_1 = x\text{-}x_a$; Fracture 2 is located at (x_b, y), such that $x_2 = x\text{-}x_b$. According to the coupled pressure superposition model, we can obtain the pressure field distribution in the reservoir from:

$$\begin{aligned} P(x,t) &= P_0 + \Delta P_0 \times \left(\left(1 - erf \frac{x_1}{2\sqrt{D_h t}}\right) + \left(1 - erf \frac{x_2}{2\sqrt{D_h t}}\right) - \left(1 - erf \frac{x_1}{2\sqrt{D_h t}}\right) \times \left(1 - erf \frac{x_2}{2\sqrt{D_h t}}\right) \right) \\ &= P_{BH} + (P_0 - P_{BH}) \times erf \frac{x_1}{2\sqrt{D_h t}} \times erf \frac{x_2}{2\sqrt{D_h t}} \end{aligned} \tag{14}$$

The physical meaning of the new pressure superposition model can be seen from Eq. (14), that is, the ratio of residual pressure caused by multiple fractures is equal to the product of the ratio of residual pressure caused by each single fracture.

Generalizing the result of Eq. (14) for any finite number n of multiple fractures, one can obtain the pressure distribution in the formation. Referenced to the initial pressure of the reservoir, Eq. (14) can be rewritten into a simpler form:

$$P(x,t) = P_0 + \Delta P_0 \left(1 - \prod_{k=1}^{n} erf \frac{x_k}{2\sqrt{D_h t}}\right) \quad (15)$$

When using a bottom-hole centered approach (Appendix A):

$$P(x,t) = P_{BH} + (P_0 - P_{BH}) \prod_{k=1}^{n} erf \frac{x_k}{2\sqrt{D_h t}} \quad (16)$$

The $P(x, t)$ according to Eq. (16) and Eq. (12) are identical. Further proof for this superposition method is given in Appendix A.

When there are multiple sources of pressure change in the reservoir region of concern, the form of Eq. (12) becomes rather complicated, so Eq. (15) is recommended for use when multiple pressure sources are involved. According to Eq. (15), we can get the Gaussian probability function of a multi-fracture reservoir from:

$$p(x,t) = 1 - \prod_{k=1}^{n} erf \frac{x_k}{2\sqrt{D_h t}} \quad (17)$$

Fig. 4 shows the pressure change probability curves near two fractures according to Eq. (14). The fracture space is 50, and D_h used is 1. As production proceeds, the dimensionless pressure change curve gradually approaches −1 from 0, and is infinitely close to −1, indicating that the reservoir pressure gradually decreases to the bottom-hole pressure.

Fig. 5 includes the pressure distribution curves given for twelve successive times (see legend), according to the traditional superposition method of Eq. (9) (dashed curves) and according to the new coupled pressure-superposition method of Eq. (15) (solid curves). During the first 100 days of production, the two types of curves basically coincide. This means that the pressure interference in the reservoir of multiple fractures (or multiple well-systems) represented by pressure transients – in the early phases of pressure advance – behaves according to the traditional superposition-method. However, after 100 days, differences begin to appear, and after 200 days the coupled pressure-superposition model solution lags behind the traditional pressure-superposition model.

Importantly, after 500 days, the reservoir pressure computed with the traditional pressure-superposition model dips below the bottom-hole pressure (and eventually becomes negative), giving increasingly physically unrealistic and inaccurate results. In contrast, the pressure distribution curve calculated by the coupled pressure-superposition model gives a realistic pressure drop. The pressure profile between the two fractures drops further over time, and asymptotically assumes the bottom-hole pressure. Our new superposition model suggests that the traditional pressure superposition model is less suitable for calculating transient pressure changes in a reservoir with superposed fractures. The same holds true for reservoirs with superposed vertical well systems, where pressure transients will interfere.

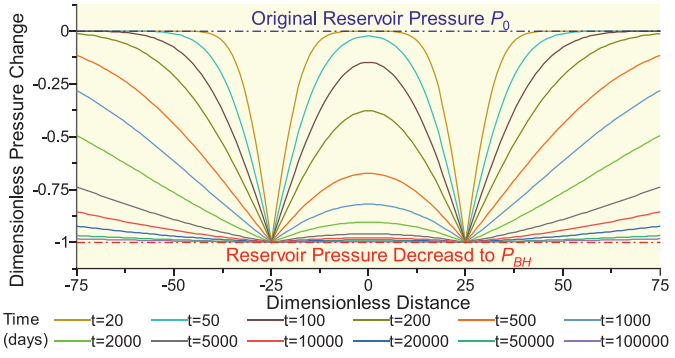


Fig. 4. Dimensionless pressure change curves for two adjacent fractures with $P_{BH} < P_0$ (production case) of the coupled pressure superposition model.

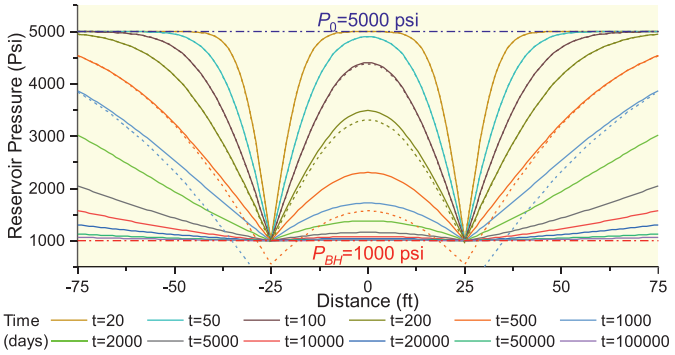


Fig. 5. Reservoir pressure distribution for reservoir space containing two hydraulic fractures placed at $x = -25$ ft and $x = +25$ ft, respectively, and spaced 50 ft.

3. Well rates solutions

Next, a practical solution scheme can be developed for the superposition of any finite number of evenly spaced planar fracture-sources in a hydraulically multi-fractured well-system (Fig. 6). The principal aim of solving for the pressure transients is to subsequently forecast the corresponding well rates.

For a single fracture case (Fig. 6a), one should use Eq. (4) as the starting point to compute the spatial and temporal pressure gradient, which has the following solution:

$$\frac{p(x,t)}{dx} = \frac{-1}{\sqrt{\pi D_h t}} e^{-\frac{x^2}{4D_h t}} \quad (18)$$

The equivalent wellhead production rate, q_{WH} (bbls/day), of this fracture ($x = 0$) follows from Darcy's Law:

$$q_{WH}(t) = \frac{kA(P_{BH} - P_0)}{\mu B} \frac{\partial p}{\partial x} = \frac{kA}{\mu B} \frac{(P_0 - P_{BH})}{\sqrt{\pi D_h t}} e^{-\frac{x^2}{4Dt}} = \frac{C_1 C_2}{C_3} 4 y_f h_f \frac{k}{\mu B} \frac{(P_0 - P_{BH})}{\sqrt{\pi D_h t}} \quad (19)$$

with the half-length, y_f (ft), of the fracture that is effectively propped, height of the reservoir corresponding to fracture height, h (ft), fluid viscosity, μ (cPoise), reservoir permeability, k (mD), initial reservoir pressure, P_0 (psi), and well-fracture system bottom-hole pressure, P_{BH} (psi), assumed constant throughout the well life. The formation volume factor, B, accounts for the fluid volume change as the fluid moves from the well system at the reservoir level to the wellhead at the surface. The factor 4 in the nominator of Eq. (19) accounts for 2-sided pressure diffusion from 2 times the fracture half-length planar surface (Fig. 6).

The conversion factor $C_1 = 0.178108$ bbls/ft^3 arises because the input units in ft on the right-hand side lead to cubic ft (per time unit), which needs conversion to oil bbls (per time unit) for the output well-rate on the right-hand side. The required conversion is 1 ft^3 = 0.178108 bbls. If we work with gas wells, the conversion factor $C_1 = 0.001$ Mcf/ft^3, because 1 ft^3 = 0.001 Mcf, and the produced gas volume will be expressed in Mcf (per time unit).

The conversion factor $C_2 = 1.06235 \times 10^{-14}$ ft^2/mD arises to convert square ft units of permeability and prorated for inputs in

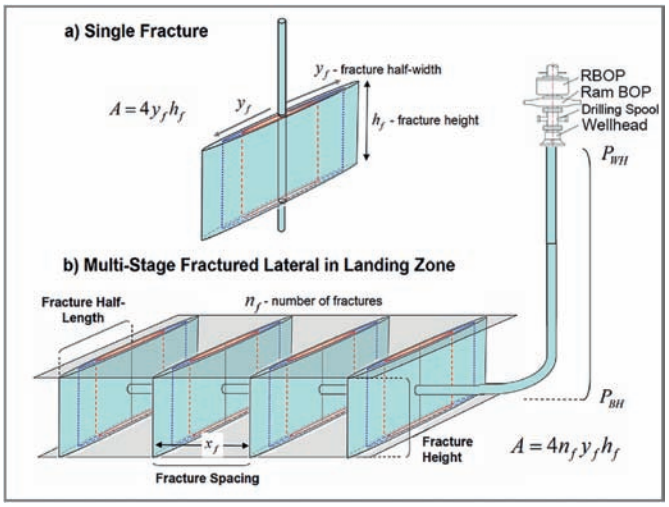


Fig. 6. Two common cases of hydraulically fractured wells are analyzed in this appendix: (a) Wells producing from a single hydraulic fracture. (b) Wells producing from multiple fractures. The surface area that acts as the pressure diffusion source is given by *A*.

mD. The required conversion factor is 1 mD = 1.06235×10^{-14} ft^2.

The conversion factor $C_3 = 1.67868 \times 10^{-12}$ psi·day/cPoise is needed if the viscosity input is in cPoise, then conversion of viscosity to psi·day will result in output for well rate in stb/day. The required conversion factor is 1 cPoise $= 1.67868 \times 10^{-12}$ psi·day.

For the multi-fractured well with n fractures, the well rate resulting from the superposed fracture sources spaced by x_f, can be computed applying the method of Eq. (16):

$$p(x,t) = \frac{\Delta P(x,t)}{\Delta P} = 1 - erf\left(\frac{x}{2\sqrt{D_h t}}\right) \times erf\left(\frac{x - x_f}{2\sqrt{D_h t}}\right) \tag{20}$$

The expression of Eq. (20) for a pair of fractures placed symmetric about the *y*-axis is:

$$p(x,t) = \frac{\Delta P(x,t)}{\Delta P} = 1 - erf\left(\frac{x - x_f/2}{2\sqrt{D_h t}}\right) \times erf\left(\frac{x + x_f/2}{2\sqrt{D_h t}}\right) \tag{21}$$

We can now translate the pressure gradient of Eq. (21) to a well rate due to cumulative fluid flowing into n number of fractures spaced at $x = \pm x_f/2$:

$$\begin{aligned} q_{WH}(t) = & \frac{C_1 C_2}{C_3} 4ny_f h_f \frac{k}{\mu B} \frac{(P_0 - P_{BH})}{\sqrt{\pi D_h t}} \\ & \times \left[e^{-\left(\frac{x - x_f/2}{2\sqrt{D_h t}}\right)^2} erf\left(\frac{x + x_f/2}{2\sqrt{D_h t}}\right) \right. \\ & \left. + e^{-\left(\frac{x + x_f/2}{2\sqrt{D_h t}}\right)^2} erf\left(\frac{x - x_f/2}{2\sqrt{D_h t}}\right) \right] \\ = & \frac{C_1 C_2}{C_3} 4ny_f h_f \frac{k}{\mu B} \frac{(P_0 - P_{BH})}{\sqrt{\pi D_h t}} erf\left(\frac{x_f}{2\sqrt{D_h t}}\right) \end{aligned} \tag{22}$$

The result of Eq. (22) is a main finding of our study, which is more accurate than prior solutions (Weijermars, 2021), now adequately accounting for pressure interference between the space fractures as their spacing becomes tighter.

A common assumption is that the hydraulic diffusivity (D_h, ft^2/day) can be computed from primary properties as follows (Weijermars, 2022; Zhang and Ayala, 2019; Zimmerman, 2018):

$$D_h = \frac{C_2}{C_3} \frac{k}{\phi \mu C_t} \tag{23}$$

Where ϕ is reservoir porosity, and C_t is total compressibility, psi^{-1}, given by $C_t = (1\text{-}\phi)C_{rock} + \phi C_{fluid}$.

Further one may choose to remove the duplicity of parameters k and μ in Eq. (22), and replace them using a theoretical expression relating the hydraulic diffusivity to primary values:

$$\begin{aligned} q_{WH}(t) = & C_1 4ny_f h_f (P_0 - P_{BH}) \frac{\phi C_t \sqrt{D_h}}{B\sqrt{\pi t}} \\ & \times \left[e^{-\left(\frac{x - x_f/2}{2\sqrt{D_h t}}\right)^2} erf\left(\frac{x + x_f/2}{2\sqrt{D_h t}}\right) \right. \\ & \left. + e^{-\left(\frac{x + x_f/2}{2\sqrt{D_h t}}\right)^2} erf\left(\frac{x - x_f/2}{2\sqrt{D_h t}}\right) \right] \\ = & C_1 4ny_f h_f (P_0 - P_{BH}) \frac{\phi C_t \sqrt{D_h}}{B\sqrt{\pi t}} erf\left(\frac{x_f}{2\sqrt{D_h t}}\right) \end{aligned} \tag{24}$$

In order to further verify our results, we compare in Section 4 the results of the coupled pressure-superposition model with those of a commercial CMG-simulator using reservoir and production data from an Eagle Ford study well in a lease region in Brazos County, East Texas.

4. Verification of coupled pressure-superposition model

The results of the new coupled GPT model are computed here with a CMG simulation applied to a case study of progressive pressure depletion in a Wolfcamp well (Neal 346AH) from the Permian Basin (Delaware Basin, West-Texas). Next, we carried out production history matching using well data from the Eagle Ford Shale (Brazos County, East Texas). The analyzed wells have been extensively studied and the pressure depletion and the drained rock volume were visualized in several prior studies using commercial simulators (Khanal and Weijermars, 2019; Weijermars et al., 2020b, 2020c; Weijermars and Khanal, 2020; Weijermars and Nascentes Alves, 2018).

4.1. Pressure curve matching

A 2014 study well (Neal 346AH, Upton County, West Texas), with a 6524 ft long lateral landed and completed in the Wolfcamp Formation, Midland Basin, was history matched and analyzed in some detail. The well is hydraulically fractured, with 60 ft perf cluster spacing assumed to originate 109 discrete hydraulic fractures with enhanced fracture conductivity (Zakhour et al., 2015). The history-matched reservoir simulation model for Neal 346AH is used here to generate pressure depletion maps and pressure depletion profiles for different times during the assumed 30-year production life of the well (Khanal et al., 2019). Although the entire well is simulated, our analysis focuses on the pressure changes near the three central fractures (no. 54–56). Focusing on the central fracture stage allows studying of the pressure depletion, at high resolution, in the matrix blocks between the individual fractures.

The initial reservoir pressure in the Wolfcamp Formation (before any production) was 5161 psi, as used in our prior history match (Khanal et al., 2019). The progression of the pressure distribution curve between the two wells was computed for 30 years using a CMG-IMEX simulator. The well dimensions, completion and formation parameters are given in Table 1. Fig. 7 shows the pressure front propagation at twelve different times from one day to thirty years of production. We can see from the pressure evolution curves that it takes only one month before adjacent fractures (spaced at 60 ft) begin to communicate with each other, in the sense that their respective pressure fronts meet. After the pressure fronts of adjacent fractures make first contact, the pressure decline around the hydraulic fractures accelerates. At the end of year 1, the bottom-hole pressure (P_{BH}) is nearly established near to the hydraulic fractures and is close to 1000 psi. The pressure saddles in the matrix blocks between the hydraulic fractures have been reduced to 2500 psi, or about half the original reservoir pressure (5161 psi). The average pressure in the grid blocks between each pair of the central fractures at year 5 has moved closer to the minimum bottom-hole pressure (1000 psi) and the pressure saddles occur at 1500 psi. After 10 years, the pressure between the fractures has basically stabilized at 1000 psi and almost no longer changes with time.

Reservoir pressure simulations based on the analytical model (Eq. (7) and Eq. (15)) critically depend on the hydraulic diffusivity. We extracted the peak pressures between two fractures and the bottom-hole pressure at different times from CMG model results (Fig. 7), and used the coupled GPT model (Eq. (15)) for curve matching (Fig. 8). By adjusting D_h and using the Pearson correlation coefficient as the matching index, the pressure evolution curve that best matches the CMG model results was obtained. The history-matching of D_h gave 2.32 ft^2/day. According to the primary parameters used in the CMG model, the theoretical $D_h = 2.51$ ft^2/day, computed from the primary parameters using Eq. (24). The close agreement between the history-matched D_h value of 2.32 ft^2/day and the primary-value-computed D_h-value of 2.51 ft^2/day affirms the accuracy and reliability of the coupled pressure superposition method.

Fig. 8 includes a curve which predicts the pressure value midpoint between the fracture pair of Fig. 7 and shows again that the traditional superposition method wrongly suggests the reservoir pressure continues to fall, eventually becoming lower than the bottom-hole pressure and even negative, which is physically unfeasible. The black solid line is the peak pressure between fractures at various times simulated by CMG, the green solid line is obtained by matching using the coupled pressure superposition method ($D_h = 2.32$ ft^2/day), and the blue solid line is obtained using the traditional pressure superposition method. The orange dotted curve is the bottom-hole pressure during the CMG simulation, which gradually decreases from 3500 psi to 1000 psi. The Pearson coefficient of 0.994 between the CMG simulation of the mid-point pressure and the coupled superposition method using the GPT method validates the accuracy of the fast analytical solutions.

Table 1
Assumed reservoir and fracture properties used to build the CMG reservoir base case model of Fig. 7.

Parameters	Values
Total Vertical Depth Well, D_w (ft)	8557
Well Length Lateral, L (ft)	6524
Number of Fractures, n	108
Fracture Spacing, x_f (ft)	60
Fracture Height, h_f (ft)	220
Fracture Half-length, y_f (ft)	105
Fracture Width, w_f (ft)	0.01
Fracture Permeability, k_f (mD)	6000
Reservoir Permeability (base case), k (nD)	100
Initial Reservoir Pressure, P_0 (psia)	5161
Reservoir Temperature, T (°F)	110
Porosity, ϕ (%)	4.2
Oil Viscosity, μ (cP)	2
Total Compressibility, C_t (psi^{-1})	3×10^{-6}

Since the CMG model and analytical model use two different calculation systems, minor mismatches may remain. For example, during the calculation process, the bottom-hole pressure in the CMG model is not constant, but decreases gradually from 3500 psi to 1000 psi. This also explains that in the early stage of production, the reservoir pressure calculated by the CMG model is slightly higher than the results adopting analytical solution method (Fig. 8). But overall, the Pearson correlation coefficient of 0.994 means the matching result is excellent.

After 10 years, the respective pressure curves based on CMG and coupled GPT history matching practically coincide, proving the reliability of the coupled GPT method. The traditional pressure superposition method would cause the reservoir pressure to continuously and significantly decrease, and will be lower than the bottom-hole pressure after one year, or even lower than −2000 psi after a decade (Fig. 8), which is obviously incorrect, which is why use of the coupled pressure superposition method of Section 2.4 is warranted.

4.2. Production curve matching

Predicting the future production curve of a hydraulically fractured well with the GPT method of Eq. (24) requires knowledge of the fracture design parameters, ny_fh_f , fracture spacing, x_f, reservoir porosity, ϕ, formation volume factor, B, and two key reservoir parameters, D_h and C_t. The latter two parameters can be obtained from measurements on core samples retrieved from pilot wells using Eq. (23), or by history matching of historic production data in nearby wells. This section will first introduce the real well data used for history matching, and the independent CMG history-matching simulation, used here to benchmark the Gaussian pressure forecasts.

4.2.1. History matching field data

The production data used in this study are from three wells in an Eagle Ford lease that was studied in considerable detail in prior studies (Weijermars and Nascentes Alves, 2018; Khanal and Weijermars, 2019; Weijermars et al., 2019). The initial pressure P_0 of the reservoir is 4891 psi, while the bottom-hole pressure is always maintained at 1000 psi. Due to the difference in the scale of fracturing, the production is various. These 3 wells are all horizontal wells with multi-stage fracturing, and the fracture information is shown in Table 2.

By matching the field production data (Fig. 9) using the GPT model with the coupled pressure superposition of Eq. (24), we obtained the hydraulic diffusivity (D_h) and total compressibility (C_t) for the reservoir region perforated by the three wells (Table 3). The history matching of the field production data using the coupled method gave an averaged Pearson correlation coefficient of 0.999 (0.9981–0.9996), and an averaged root mean square error (RMSE) of 0.0109 (0.0069–0.016), which proves the superb model matching accuracy.

Moreover, we found that the D_h and C_t obtained by matching the production data of each of the three wells are very similar (Table 3). According to Eq. (23), we can also get the value D_h and a comprehensive reservoir characterization parameter ($k/\phi\mu$), which also have similar values for each of the three wells (Table 3).

4.2.2. History matching CMG model outputs

There is operational noise (workover days, shut in) in the field

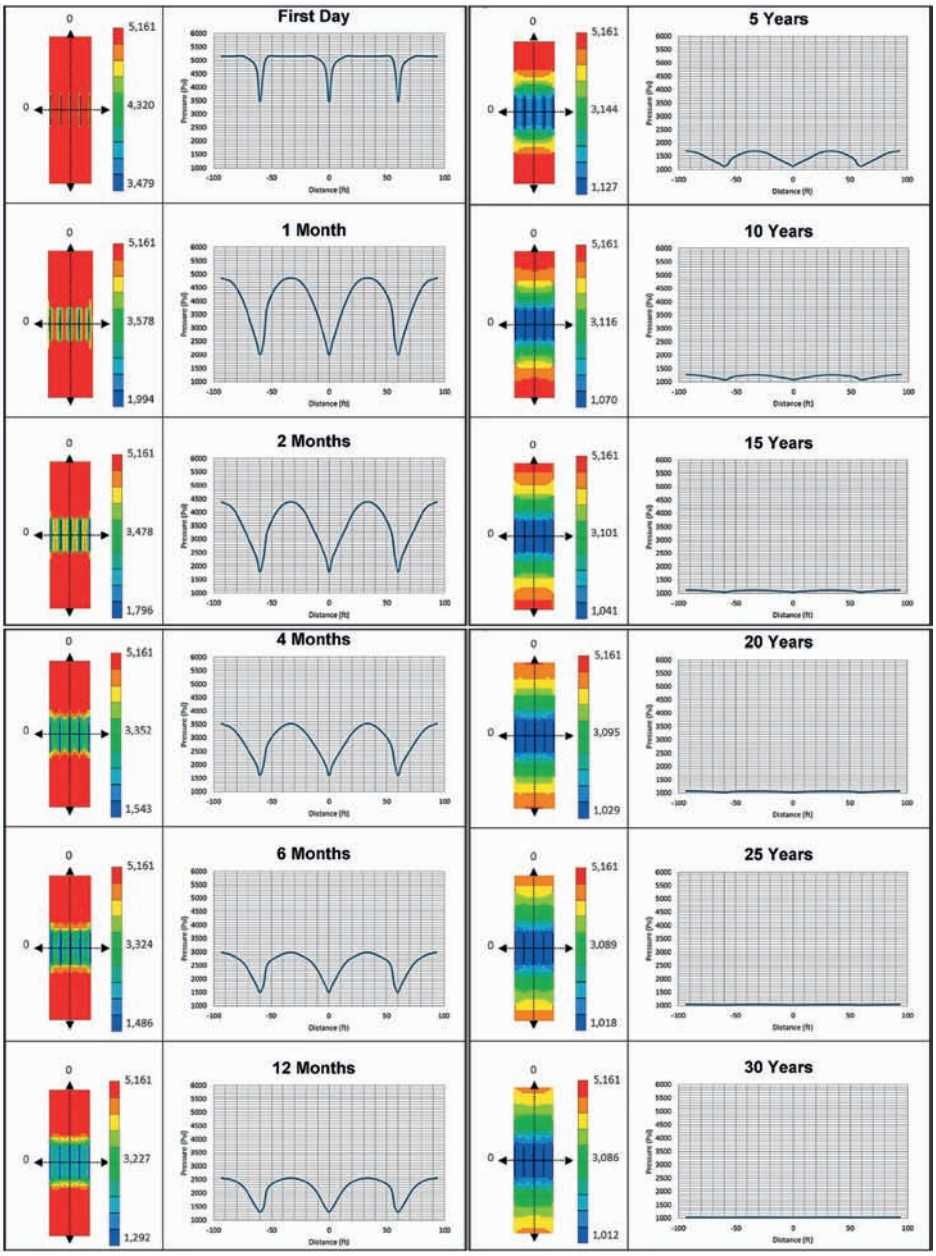


Fig. 7. Thirty years pressure depletion (psi) progression for the central 3 fractures in Neal 346AH, a Wolfcamp shale well (Midland Basin, West Texas) constructed using a production history-matched CMG model. Left column: Map views of pressure depletion in production bench with wellbore horizontal in image and transverse fractures sets spaced at 60 ft. Right column: pressure distribution normal to the fractures (Khanal et al., 2019).

data, which is why we also use noise-free production curves obtained using a CMG reservoir simulator. The CMG reservoir simulator data matched the wells in multiple realizations and was used here to also provide product curves for cases using larger and smaller fracture spacing, relative to the 60 ft spacing used in the actual completion program for the Eagle Ford legacy wells studied (Weijermars et al., 2020b). The number of fractures is determined by well length and perforation cluster spacing; smaller fracture spacing means a higher number of fractures was used. The corresponding production curves are shown in Fig. 10.

Using the Gaussian solution of Eq. (24) to history match the suite of synthetic cumulative production curves obtained from the CMG simulation for each fracture spacing in Fig. 10, D_h and C_t were obtained (dotted lines in Fig. 11). Judging from Pearson correlation coefficient and root mean square error (RMSE) matches, the narrower fracture spacing gives outstanding matches (with RMSE of 0.0179 and Pearson coefficient of 0.9959). For the largest fracture spacing evaluated (100 ft), the fit is more outstanding (with RMSE of 0.0088 and Pearson coefficient of 0.9994).

4.2.3. Reservoir characterization

The D_h and C_t used for each curve in Fig. 11 are listed in Table 4, and the variation trends of parameters with fracture spacing are graphed in Fig. 12. For fracture spacing less than 50 ft, D_h increases significantly. The D_h obtained when the fracture spacing is 30 ft is more than twice ($D_h = 4.2$ ft^2/day) than the result for the 50 ft fracture spacing ($D_h = 1.8$ ft^2/day). When the fracture spacing exceeds 50 ft, D_h barely changes (ranging between 1.5 and 1.8 ft^2/day).

However, the estimated C_t-values first increase when fracture spacing increases. Separately, the comprehensive reservoir characterization parameter ($k/\phi\mu$) shows an increase as fracture

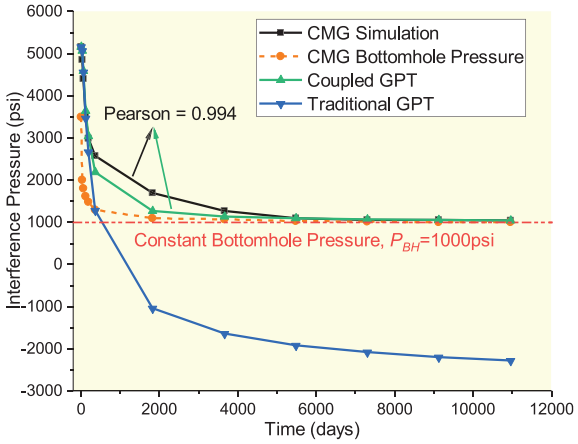


Fig. 8. Matching curves of pressure evolution within 30 years.

Table 2
Fracture information of 3 Eagle Ford study wells.

Parameter	Well R	Well H	Well M
Well length lateral, L (ft)	8630	6550	5950
Fracture spacing, x_f (ft)	63	50	50
Fracture half-length, y_f (ft)	215	144	137
Fracture height, h (ft)	60	60	60
Fracture number, n	139	131	119
Initial reservoir pressure, P_0 (psi)		4891	
Bottom-hole pressure, P_{BH} (psi)		1000	
Reservoir Permeability, k (nD)		150	
Porosity, ϕ		0.05	
Oil Viscosity, μ (cP)		2	
Total Compressibility, C_t (psi^{-1})		3×10^{-6}	
Volume factor, B		1.2	

spacing gets tighter (red curve in Fig. 12). The escalation effect of higher diffusivity for tighter fracture spacing is here ascribed to either a decrease in porosity or increase in permeability, or both (see discussion in Section 5.3).

5. Discussion

Based on the coupled Gaussian model, we obtained accurate solutions for the transient pressure field changes between hydraulic fractures, and calculated the production based on the pressure gradient. The results obtained by the coupled-GPT model and the CMG simulator both were matched against real well data and showed outstanding matches. This study has achieved scientific progress with significant practical value for analytical production forecasting and shale well performance optimization. In particular, engineering solutions will benefit from three main findings as highlighted in Sections 5.1 to 5.3.

5.1. Pressure superposition improvement

Using the traditional superposition model, the reservoir pressure could become lower than the bottom-hole pressure, or even negative. This is because the traditional pressure superposition model is only applicable to steady-state pressure fields, that is, it describes the pressure field theoretically required for a constant flow state. However, this state is impossible for an infinitely large reservoir unless there is an aquifer resupply source. For an infinitely large reservoir, maintaining a constant production rate is impossible because the bottom-hole pressure cannot be reduced perpetually. When the bottom-hole pressure gradient advances into the reservoir, there occurs a limit for which the pressure gradient will no longer provide sufficient gradient near the well to maintain substantial flow. Over time, the well rate will asymptotically decline and reach the bottom-hole pressure imposed by the well's production system, until the production rate will cease altogether.

The coupled GPT model considers the interference of the transient pressure fields between multiple wells or fractures. The transient changes in the reservoir pressure will affect the production or injection rate of any well; such wells cannot flow in steady-state. The model calculation results show that the newly proposed coupled GPT model can obtain a reservoir pressure distribution that matches the physical conditions. Its accuracy and reliability were confirmed by benchmarking against CMG simulation results.

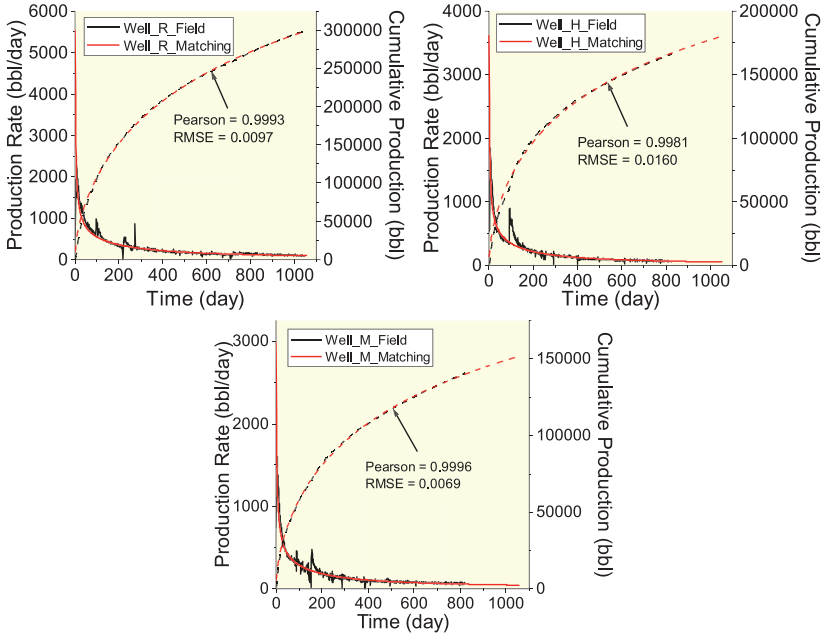


Fig. 9. Field production data and historical matching results of three study wells (Well_R, Well_H, Well_M).

Table 3
Reservoir parameters obtained by history matching.

Well Names	D_h (Eq. (23))	D_h	C_t	$D_h \times C_t = k/\phi\mu$
	ft^2/day	ft^2/day	1×10^{-5} psi^{-1}	$(1 \times 10^{-5}$ $ft^2day^{-1}psi^{-1})$
Well_R	3.167	3.24	2.626	8.507
Well_H		3.128	2.759	8.631
Well_M		2.846	2.762	7.859
Average		3.071	2.716	8.332

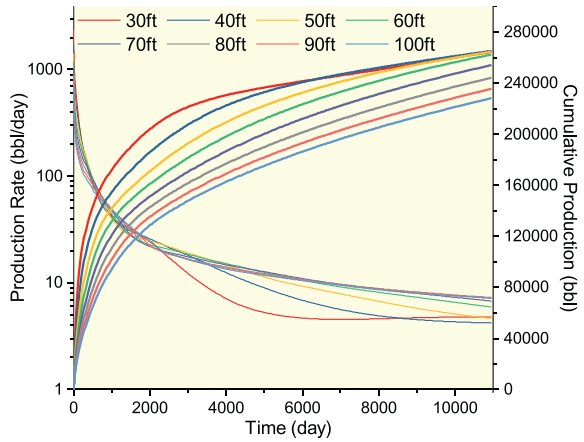


Fig. 10. Production curves for different fracture spacing simulated by CMG.

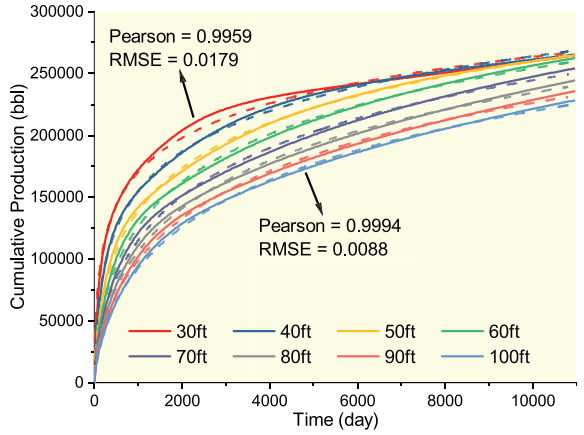


Fig. 11. Matching results of production curves for different fracture spacing. The solid line is the result of CMG simulation, and the dotted line is the result of matching.

5.2. Production forecasting improvement

Based on the coupled GPT model, we obtained an analytical expression for the pressure gradient around the individual fractures, and obtained the fluid flow rate and wellhead production according to Darcy's law. According to the history matching of three independent wells in the same reservoir, we found that the D_h, C_t and $k/\phi\mu$ of the three wells closely matched. Additionally, the empirical D_h-values were approximately the same as the values calculated from primary reservoir parameters using the theoretical result of Eq. (23) (Table 3), which further supports the validity and accuracy of the coupled GPT model in forecasting future well production rates.

5.3. Reservoir characterization merits

We used the coupled GPT model for history matching production curves considering various fracture spacings. When the fracture spacing is tight (≤40 ft), the equivalent D_h increases significantly, while the C_t gradually decreases. In the classical pressure transient analysis, D_h is assumed to be a constant (Raghaven, 1993). However, Zhang and Ayala pointed out that when the reservoir is going through significant depletion, the pressure dependence of the D_h cannot be ignored (Zhang and Ayala, 2019). In this study, the small fracture spacing resulted in faster pressure depletion between fractures, which in turn resulted in significant changes in the history matched D_h. Since the D_h is a composite parameter, jointly controlled by multiple parameters, we calculated the $k/\phi\mu$ of the reservoir according to Eq. (23). Assuming that the fluid viscosity (μ) remains unchanged, we see that when the fracture spacing decreases, the fluid flow capacity in the SRV area is enhanced, and the equivalent permeability (k) increases, or the porosity (ϕ) of the reservoir decreases, or both.

Table 4
Reservoir parameters obtained by history matching with various fracture spacing.

Fracture Space	D_h (Eq. (23))	D_h	C_t	$D_h \times C_t = k/\phi\mu$
	ft^2/day	ft^2/day	1×10^{-5} psi^{-1}	$(1 \times 10^{-5}$ $ft^2day^{-1}psi^{-1})$
x_f_30	1.637	4.192	1.896	7.95
x_f_40		2.483	2.27	5.636
x_f_50		1.806	2.584	4.668
x_f_60		1.603	2.802	4.492
x_f_70		1.568	2.908	4.56
x_f_80		1.644	2.94	4.833
x_f_90		1.699	2.987	5.074
x_f_100		1.729	3.052	5.277

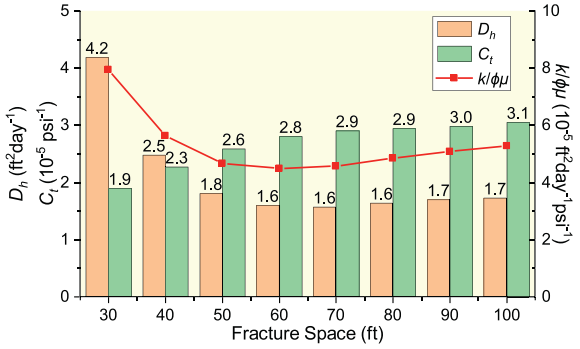


Fig. 12. The changing trend of equivalent reservoir properties for various fracture spaces.

5.4. Strengths and weaknesses

The coupled GPT model can quickly calculate the pressure field distribution and production curve of MFHW using only basic reservoir parameters, and has considerable practical value. The current coupled GPT model can be further improved in two obvious domains: (1) When calculating the pressure field distribution, if multiple wells are used and some infill wells disturb the pressure field at a later time, then the initiation time (t) in the coupled GPT model need to be corrected. (2) When calculating the production, only the production of linear flow on both sides of the fracture is included, while the production of radial flow at the fracture tip is ignored. This is because the transient pressure field distribution equation for radial flow in a single well with constant bottom-hole pressure was only recently solved (Weijermars and Afagwu, 2024). However, the contribution of the fracture tip to the total production can be ignored in the early stage of production; only when the time is long enough for the pressure in the SRV area to be nearly exhausted, the fracture tip will make a significant contribution to the production rate (Tian and Weijermars, 2024). If the pressure field distribution between wells can be obtained based on the coupled pressure superposition

model, the accuracy of the coupled GPT model in predicting the production curve can be further improved.

6. Conclusions

This paper studies the pressure field evolution of MFHW and points out the limitations of the traditional pressure superposition model. The coupled GPT model based on the coupled pressure superposition model shows significant advantages in pressure calculation and production prediction of multi-fracture systems. The main conclusions are as follows:

(1) The traditional pressure superposition method will produce unreasonable pressure when running for a long time. The newly proposed coupled pressure superposition method improves the calculation accuracy of the pressure field by introducing a correction coefficient. Its application in multi-fracture systems shows higher accuracy.
(2) Based on the closed-form solution, the GPT method provides a fast calculation tool for forecasting well rates even prior to drilling; the pressure field is resolved with infinite resolution as no gridding is involved. Compared with numerical simulation methods, the coupled GPT model has obvious advantages in calculation speed and accuracy, and is particularly suitable for data iteration and history matching in the early stage of reservoir development.
(3) For MFHW, the matching results show that as the fracture spacing decreases, the hydraulic diffusion coefficient (D_h) and the equivalent permeability (k) in the SRV region increase, and the equivalent porosity (ϕ) decreases. The Gaussian GPT method can be used as a practical tool for reservoir characterization.

CRediT authorship contribution statement

Yakai Tian: Writing – original draft, Visualization, Validation, Methodology, Investigation, Data curation. **Ruud Weijermars:** Writing – review & editing, Supervision, Investigation, Formal analysis, Conceptualization.

Declaration of competing interest

The authors declare that they have no known competing financial interests or personal relationships that could have appeared to influence the work reported in this paper.

Acknowledgment

The authors acknowledge the generous support provided by the College of Petroleum Engineering & Geosciences (CPG) at King Fahd University of Petroleum & Minerals (KFUPM).

Appendix A. Proof of Pressure Superposition for Transient Flow of Multi-Fracture Systems

We adopt a representation of the spatial pressure-change over time by a pressure-transient probability density function (Eq. (8)):

$$\Delta P(x_k, t_k) = (P_{BH} - P_0)\left(1 - erf\left(\frac{x_k}{2\sqrt{D_h t_k}}\right)\right) \tag{A1}$$

Where $\left(1 - erf\left(\frac{x_k}{2\sqrt{D_h t_k}}\right)\right)$ is the ratio of the pressure drop caused by the fracture k (Crank, 1975; Weijermars, 2022).

Eq. (9) in the main text is only applicable to steady-state seepage conditions, and assumes that the pressure change at a point in the formation is ultimately becomes equal to the superposition of the pressure changes of all fractures at that point. As for the unsteady or transient pressure change conditions, this paper puts forward a new solution according to Eq. (12): the pressure change caused by a fracture depends on the pressure difference between the bottom-hole and the formation.

The hydraulic diffusivity, D_h, captures the intrinsic properties of the reservoir and as all the fractures are supposed to interfere in the same reservoir, we do not assume any variation in diffusivity between fractures. An instantaneously applied bottomhole pressure, P_{BH}, is assumed to be held constant in the well and its hydraulic fractures throughout the production period. If all fractures have the same P_{BH} and start operating at the same time, t.

If only fracture 1 exists, the pressure distribution in the formation at time t is (in a bottomhole centered approach):

$$\begin{aligned} P_1 &= P_0 + (P_{BH} - P_0) \times \left(1 - erf\left(\frac{x_1}{2\sqrt{D_h t}}\right)\right) \\ &= P_{BH} + (P_0 - P_{BH}) \times erf\left(\frac{x_1}{2\sqrt{D_h t}}\right) \end{aligned} \tag{A2}$$

If two fractures exist at the same time, considering the interference between fracture 1 and 2, we obtain the pressure distribution in the formation according to Eq. (14):

$$P_{1+2} = P_{BH} + (P_0 - P_{BH}) \times erf\left(\frac{x_1}{2\sqrt{D_h t}}\right) \times erf\left(\frac{x_2}{2\sqrt{D_h t}}\right) \tag{A3}$$

If there are 3 fractures, the pressure distribution in the formation according to Eq. (12) is:

$$\begin{aligned} P_{1+2+3} &= P_0 + \Delta P_0 \times \left(\begin{array}{l} \left(1 - erf\frac{x_1}{2\sqrt{D_h t}} erf\frac{x_2}{2\sqrt{D_h t}}\right) + \left(1 - erf\frac{x_3}{2\sqrt{D_h t}}\right) \\ -\left(1 - erf\frac{x_1}{2\sqrt{D_h t}} erf\frac{x_2}{2\sqrt{D_h t}}\right) \times \left(1 - erf\frac{x_3}{2\sqrt{D_h t}}\right) \end{array} \right) \\ &= P_{BH} + (P_0 - P_{BH}) \times erf\left(\frac{x_1}{2\sqrt{D_h t}}\right) \times erf\left(\frac{x_2}{2\sqrt{D_h t}}\right) \times erf\left(\frac{x_3}{2\sqrt{D_h t}}\right) \end{aligned} \tag{A4}$$

Similarly, for multiple fractures, based on Eq. (12), we can obtain the pressure distribution (in an initial reservoir pressure centered approach):

$$P(x,t) = P_{BH} + (P_0 - P_{BH}) \prod_{k=1}^{n} erf\left(\frac{x_k}{2\sqrt{D_h t}}\right) \quad \text{(A5)}$$

The solution of Eq. (A5) is given in Eq. (16) and the proof given in this appendix shows that both Eqs. (12) and (16) are in fact mathematically identical, but were derived using, respectively, bottomhole and initial reservoir pressure centered approaches.

References

Afagwu, C., Al-Afnan, S., Abdalla, M., Weijermars, R., 2024. Gaussian pressure-transients: a toolkit for production forecasts and optimization of multi-fractured well systems in shale formations. Arabian J. Sci. Eng. https://doi.org/10.1007/s13369-024-08921-x.

Alotaibi, M., Alotaibi, S., Weijermars, R., 2023. Stream and potential functions for transient flow simulations in porous media with pressure-controlled well systems. Fluid 8, 160. https://doi.org/10.3390/fluids8050160.

Alvestad, J., 2021. Open Porous Media Flow Reference Manual, Rev-1. Equinor ASA.

Bai, W., Cheng, S., Wang, Y., Cai, D., Guo, X., Guo, Q., 2024. A transient production prediction method for tight condensate gas wells with multiphase flow. Petrol. Explor. Dev. 51, 172–179. https://doi.org/10.1016/S1876-3804(24)60014-5.

Brown, M., Ozkan, E., Raghavan, R., Kazemi, H., 2011. Practical solutions for pressure transient responses of fractured horizontal wells in unconventional reservoirs. SPE Reservoir Eval. Eng. 14 (6), 663–676.

Clarkson, C.R., 2012. Production data analysis of unconventional gas wells: Review of theory and best practices. J. Petrol. Sci. Eng. 23, 101–146. https://doi.org/10.1016/j.coal.2013.01.002.

Crank, J., 1975. The Mathematics of Diffusion, 2nd ed. Oxford University Press.

Fanchi, J.R., Harpole, K.J., Bujnowski, S.W., 1982. BOAST: a three-dimensional, three-phase black oil applied simulation tool (version 1. 1). Technical Description and Fortran Code (No. DOE/BC/10033-3). Keplinger and Associates, Inc., Tulsa, OK (USA); BDM Corp., Bartlesville, OK (USA).

Feynman, R., 1952. Negative probability. Available from CERN-server. https://cds.cern.ch/record/154856/files/pre-27827.pdf/.

Guo, J., Li, M., Zhuang, M., Sun, Y., 2023. Rock physics model for velocity—pressure relations and its application to shale pore pressure estimation. Petrol. Explor. Dev. 50, 404–418. https://doi.org/10.1016/S1876-3804(23)60396-9.

Ji, J., Yao, Y., Huang, S., Ma, X., Zhang, S., Zhang, F., 2023. Production-induced pressure-depletion and stress anisotropy changes near hydraulically fractured wells: implications for intra-well fracture interference and fracturing treatment efficacy. Int. J. Coal Geol. 222, 211450. https://doi.org/10.1016/j.geoen.2023.211450.

Ji, J., Yao, Y., Huang, S., Ma, X., Zhang, S., Zhang, F., 2017. Analytical model for production performance analysis of multi-fractured horizontal well in tight oil reservoirs. J. Petrol. Sci. Eng. 158, 380–397. https://doi.org/10.1016/j.petrol.2017.08.037.

Khanal, A., Nandlal, K., Weijermars, R., 2019. Impact of natural fractures on the shape and location of drained rock volumes in unconventional reservoirs: case studies from the Permian Basin. In: Proceedings of the 7th Unconventional Resources Technology Conference. American Association of Petroleum Geologists, Denver, Colorado, USA. https://doi.org/10.15530/urtec-2019-1082.

Khanal, A., Weijermars, R., 2019. Pressure depletion and drained rock volume near hydraulically fractured parent and child wells. J. Petrol. Sci. Eng. 172, 607–626. https://doi.org/10.1016/j.petrol.2018.09.070.

Lee, S.T., Brockenbrough, J.R., 1988. A new approximate analytic solution for finite conductivity vertical fractures. Form. Eval 1 (1), 75–88.

Lei, Z., Wang, Z., Mu, L., Peng, H., Li, X., Bai, X., Tao, Z., Li, H., Peng, Y., 2024. A technique for enhancing tight oil recovery by multi-field reconstruction and combined displacement and imbibition. Petrol. Explor. Dev. 51, 152–163. https://doi.org/10.1016/S1876-3804(24)60012-1.

Lie, K.-A., 2019. An Introduction to Reservoir Simulation Using MATLAB/GNU Octave: User Guide for the MATLAB Reservoir Simulation Toolbox (MRST). Cambridge University Press.

Nandlal, K., Li, C., Liu, C.-H., Chavali, V.B.K., King, M.J., Weijermars, R., 2020. Understanding field performance of hydraulically fractured wells: Comparison of pressure front versus tracer front propagation using the Fast Marching Method (FMM) and Complex Analysis Method (CAM). In: Proceedings of the 8th Unconventional Resources Technology Conference. American Association of Petroleum Geologists. https://doi.org/10.15530/urtec-2020-2474. Online.

Parsegov, S.G., Nandlal, K., Schechter, D.S., Weijermars, R., 2018. Physics-driven optimization of drained rock volume for multistage fracturing: field example from the wolfcamp formation, Midland Basin. In: Proceedings of the 6th Unconventional Resources Technology Conference. American Association of Petroleum Geologists, Houston, Texas, USA. https://doi.org/10.15530/urtec-2018-2879159.

Raghaven, R., 1993. Well Test Analysis. Englewood Cliffs, Prentice-Hall.

Stalgorova, E., Mattar, L., 2012. Practical analytical model to simulate production of horizontal wells with branch fractures. In: SPE Canadian Unconventional Resources Conference. OnePetro. https://doi.org/10.2118/162515-MS.

Tian, Y., Weijermars, R., 2024. Production forecasting and history matching of hydraulically fractured reservoirs using a Pressure Depletion Volume (PDV) method. In: International Petroleum Technology Conference. OnePetro. https://doi.org/10.2523/IPTC-23764-MS.

Van Harmelen, A., Weijermars, R., 2018. Complex analytical solutions for flow in hydraulically fractured hydrocarbon reservoirs with and without natural fractures. Appl. Math. Model. 56, 137–157. https://doi.org/10.1016/j.apm.2017.11.027.

Wang, J., Li, C., Sun, J., Tang, L., Zhong, R., Liu, X., Zheng, S., 2022. An analysis method of injection and production dynamic transient flow in a gas field storage facility. Petrol. Explor. Dev. 49, 179–190. https://doi.org/10.1016/S1876-3804(22)60014-4.

Wang, J., Weijermars, R., 2021. Stress anisotropy changes near hydraulically fractured wells due to production-induced pressure-depletion. In: ARMA/DGS/SEG International Geomechanics Symposium. OnePetro.

Wang, Y., Yu, H., Zhang, J., Feng, N., Cheng, S., 2023. Transient pressure analysis of polymer flooding fractured wells with oil-water two-phase flow. Petrol. Explor. Dev. 50, 175–182. https://doi.org/10.1016/S1876-3804(22)60378-1.

Waters, D., Weijermars, R., 2021. Predicting the performance of undeveloped multi-fractured marcellus gas wells using an analytical flow-cell model (FCM). Energies 14, 1734. https://doi.org/10.3390/en14061734.

Weijermars, R., 2022. Production rate of multi-fractured wells modeled with Gaussian pressure transients. J. Petrol. Sci. Eng. 210, 110027. https://doi.org/10.1016/j.petrol.2021.110027.

Weijermars, R., 2021. Diffusive mass transfer and Gaussian pressure transient solutions for porous media. Fluid 6, 379. https://doi.org/10.3390/fluids6110379.

Weijermars, R., Afagwu, C., 2024. Pressure transient solutions for unbounded and bounded reservoirs produced and/or injected via vertical well systems with constant bottomhole pressure. Fluid 9, 199. https://doi.org/10.3390/fluids9090199.

Weijermars, R., Afagwu, C., 2022. Hydraulic diffusivity estimations for US shale gas reservoirs with Gaussian method: implications for pore-scale diffusion processes in underground repositories. J. Nat. Gas Sci. Eng. 106, 104682. https://doi.org/10.1016/j.jngse.2022.104682.

Weijermars, R., Khanal, A., 2020. Flow in fractured porous media modeled in closed-form: augmentation of prior solution and side-stepping inconvenient branch cut locations. Fluid 5, 51. https://doi.org/10.3390/fluids5020051.

Weijermars, R., Khanal, A., 2019. High-resolution streamline models of flow in fractured porous media using discrete fractures: implications for upscaling of permeability anisotropy. Earth Sci. Rev. 194, 399–448. https://doi.org/10.1016/j.earscirev.2019.03.011.

Weijermars, R., Khanal, A., Zuo, L., 2020a. Fast models of hydrocarbon migration paths and pressure depletion based on Complex Analysis Methods (CAM): mini-review and verification. Fluid 5, 7. https://doi.org/10.3390/fluids5010007.

Weijermars, R., Nandlal, K., Khanal, A., Tugan, M.F., 2019. Comparison of pressure front with tracer front advance and principal flow regimes in hydraulically fractured wells in unconventional reservoirs. J. Petrol. Sci. Eng. 183, 106407. https://doi.org/10.1016/j.petrol.2019.106407.

Weijermars, R., Nascentes Alves, I., 2018. High-resolution visualization of flow velocities near frac-tips and flow interference of multi-fracked Eagle Ford wells, Brazos County, Texas. J. Petrol. Sci. Eng. 165, 946–961. https://doi.org/10.1016/j.petrol.2018.02.033.

Weijermars, R., Pham, T., Stegent, N., Dusterhoft, R., 2020c. Hydraulic fracture propagation paths modeled using Time-Stepped Linear Superposition Method (TLSM): application to fracture treatment stages with interacting hydraulic and natural fractures at the wolfcamp field test site (HFTS). In: 54th U.S. Rock Mechanics/Geomechanics Symposium. OnePetro.

Weijermars, R., Tugan, M.F., Khanal, A., 2020b. Production rates and EUR forecasts for interfering parent-parent wells and parent-child wells: fast analytical solutions and validation with numerical reservoir simulators. J. Petrol. Sci. Eng. 190, 107032. https://doi.org/10.1016/j.petrol.2020.107032.

Yu, W., Xing, Y., Cheng, M., Chen, P., Fiallos, T., Mauricio, X., Mao, Z., Miao, J., 2021. Different numerical methods for naturally fractured reservoir simulation with EDFM. In: 55th U.S. Rock Mechanics/Geomechanics Symposium, OnePetro.

Yuan, B., Su, Y., Moghanloo, R.G., Rui, Z., Wang, W., Shang, Y., 2012. A new analytical multi-linear solution for gas flow toward fractured horizontal wells with different fracture intensity. J. Petrol. Sci. Eng. 23, 227–238. https://doi.org/10.1016/j.jngse.2015.01.045.

Zakhour, N., Shoemaker, M., Lee, D., 2015. Integrated workflow using 3D seismic and geomechanical properties with microseismic and stimulation data to optimize completion methodologies: wolfcamp shale-oil play case study in the Midland Basin. In: SPE Eastern Regional Meeting, SPE, Morgantown, West Virginia, USA. https://doi.org/10.2118/177298-MS. SPE-177298-MS.

Zhang, D., Zhang, L., Tang, H., Zhao, Y., 2022. Fully coupled fluid-solid productivity numerical simulation of multistage fractured horizontal well in tight oil reservoirs. Petrol. Explor. Dev. 49, 382–393. https://doi.org/10.1016/S1876-3804(22)60032-6.

Zhang, M., Ayala, L.F., 2019. Application of superposition principle to variable rate/pressure production analysis of multi-fractured horizontal wells in unconventional gas reservoirs. J. Nat. Gas Sci. Eng. 72, 103011. https://doi.org/10.1016/j.jngse.2019.103011.

Zimmerman, R.W., 2018. The Imperial College Lectures in Petroleum Engineering: Volume 5: Fluid Flow in Porous Media. WORLD SCIENTIFIC (EUROPE).